Heliyon 10 (2024) e29005

Contents lists available at ScienceDirect

Heliyon

journal homepage: www.cell.com/heliyon

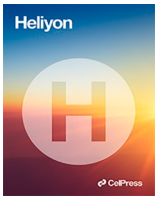

Research article

Disulfidptosis-related lncRNA signature reveals immune microenvironment and novel molecular subtyping of stomach adenocarcinoma

Jinze Li [a,b,1], Chuqi Xia [a,1], Yilin Song [c,1], Lu Zhang [a], Wei Shang [d], Ning Xu [a,**], Qiyu Lu [a,***], Daoming Liang [a,*]

[a] Second Affiliated Hospital of Kunming Medical University, Kunming, Yunnan Province, 650106, PR China
[b] Department of Gastrointestinal surgery, The Third People's Hospital of Hubei Province, Wuhan, 430071, PR China
[c] Shantou university medical college, 22 xinling Road, Shantou, Guangdong Province, 515041, PR China
[d] Shiyan People's Hospital of Hubei Medical College, Shi Yan, Hubei Province, 442000, PR China

ARTICLE INFO

Keywords:
Disulfidptosis
Stomach cancer
Chemosensitivity
Tumor immune microenvironment
Tumor subtype

ABSTRACT

The main challenge in treating stomach adenocarcinoma (STAD) is chemotherapy resistance, which is characterized by changes in the immune microenvironment. Disulfidptosis, a novel form of programmed cell death, is involved in STAD but its mechanism is not fully understood. Long non-coding RNAs (LncRNAs) may play a role in regulating disulfidptosis and influencing the immune microenvironment and chemotherapy resistance in STAD. This study aims to establish disulfidptosis-related lncRNA (DRL) features and explore their significance in the immune microenvironment and chemotherapy resistance in STAD patients. By analyzing RNA sequencing and clinical data from STAD patients and extracting disulfidptosis-related genes, we identified DRLs through co-expression, single-factor and multi-factor Cox regression, and Lasso regression analyses. We also investigated differences in the immune microenvironment, immune function, immune checkpoint gene expression, and chemotherapy resistance between different risk groups using various algorithms. A prognostic risk model consisting of 2 DRLs was constructed, with a strong predictive value for patient survival, outperforming other clinical-pathological factors in predicting 3-year and 5-year survival. Immune-related analysis revealed a strong positive correlation between T cell $CD4^+$ cells and risk score across all algorithms, and higher expression of immune checkpoint genes in the high-risk group. In addition, high-risk patients showed better sensitivity to Erlotinib, Oxaliplatin, and Gefitinib. Furthermore, three novel molecular subtypes of STAD were identified based on the 2-DRLs features, with evaluation of the immune microenvironment and chemotherapy drug sensitivity for each subgroup, which holds significant implications for achieving precise treatment in STAD. Overall, our 2-DRLs prognostic model demonstrates high predictive value for patient survival in STAD, potentially providing new targets for individualized immune and chemical therapy.

* Corresponding author.
** Corresponding author.
*** Corresponding author.
E-mail addresses: 20221106@kmmu.edu.cn (J. Li), 20231961@kmmu.edu.cn (C. Xia), 20ylsong@stu.edu.cn (Y. Song), zhanglu1@kmmu.edu.cn (L. Zhang), weishang@hbmu.edu.cn (W. Shang), xuning@kmmu.edu.cn (N. Xu), luqiyu@kmmu.edu.cn (Q. Lu), liangdaoming@kmmu.edu.cn (D. Liang).
[1] these authors made equal contributions.

https://doi.org/10.1016/j.heliyon.2024.e29005
Received 5 November 2023; Received in revised form 25 March 2024; Accepted 28 March 2024
Available online 9 April 2024

1. Introduction

Gastric cancer, or stomach cancer, specifically stomach adenocarcinoma (STAD), poses a significant public health risk [1,2]. It is the fifth most common cancer worldwide and the third leading cause of cancer-related deaths [3]. In 2018, there were over 1,000,000 new cases and an estimated 783,000 deaths. Chemotherapy remains the primary treatment for postoperative or advanced gastric cancer, as it can reduce recurrence, prolong survival, and improve quality of life [4]. However, the increasing resistance to chemotherapy greatly limits its effectiveness and may lead to treatment failure [1]. Therefore, there is an urgent need to study the specific mechanisms of drug resistance and find solutions in a clinical setting.

Disulfides are stable compounds that maintain protein structure through inter- and intra-subunit crosslinking [5]. Excessive accumulation of disulfides can lead to a form of programmed cell death called "disulfide catastrophe" [6]. High expression of SLC7A11 in glucose-deprived conditions triggers disulfide stress and cell death [7]. This form of cell death is distinct from apoptosis and ferroptosis, and can be enhanced by thiol oxidizing agents like disulfiram [5]. Disulfide catastrophe may offer new avenues for tumor treatment and can influence immune infiltration [5]. Further research is needed to identify biomarkers and explore the underlying mechanisms and therapeutic implications.

Recent findings show a close link between disulfide metabolism and cancer. Disruption of disulfide metabolism in cancer cells affects survival, proliferation, drug resistance, metastasis, and immune evasion [8–10]. Disulfide catastrophe, a form of programmed cell death, may be related to tumor immune response. It activates tumor-specific T cell immune response and enhances cancer treatment efficacy [5]. However, the relationship between disulfide catastrophe and gastric cancer, particularly in chemotherapy resistance and immune microenvironment modulation, requires further investigation. Identification of biomarkers and understanding the connection between disulfide metabolism and gastric cancer is needed.

Significant progress has been made in recent years in optimizing delivery strategies and chemical modification technologies for targeting lncRNAs, including the utilization of polymers, lipid nanoparticles, and extracellular vesicles (EXs) [11,12]. These approaches for lncRNA targeting have proven to be more accessible and efficient compared to the development of specific protein binding inhibitors [11,12]. Therefore, the discovery of lncRNA biomarkers in gastric cancer holds even greater potential, as it can easily translate into effective targets for clinical application.

Our focus was to investigate the role of disulfidptosis in STAD and its relationship with chemotherapy resistance and the immune microenvironment. Through co-expression, single-factor and multi-factor Cox regression, and Lasso regression analyses, we identified disulfidptosis-related lncRNAs (DRLs). We evaluated the immune microenvironment and drug resistance in different risk groups. Furthermore, using the 2-DRLs model, we classified STAD samples into three molecular subtypes to assist clinicians in making personalized treatment decisions. Our study suggests that DRLs hold promise as effective targets for the diagnosis and treatment of STAD. The risk prognostic model and gene subtypes provide new perspectives for precision immune therapy and clinical decision-making in STAD.

2. Materials and methods

2.1. Data collection and preprocessing

We have acquired the TCGA-STAD dataset, encompassing transcriptomic data from 408 patients diagnosed with gastric cancer, which used for differential analysis. Out of these patients, 371 samples possess complete survival information for subsequent survival and clinical analysis. The transcriptomic data underwent log2 transformation in order to standardize the gene expression data within each sample [13]. By utilizing Ensembl's annotation file, we successfully extracted the expression levels of both mRNA and lncRNA genes. This study strictly adheres to all guidelines outlined by TCGA. Moreover, we meticulously handpicked previous published experimental studies [6,7,14] to summarize 24 significant genes associated with disulfidptosis (refer to Table S1). Employing Pearson correlation analysis, we further employed stringent criteria (correlation coefficient >0.5 and p-value <0.001) to narrow down the pool of disulfidptosis-related lncRNAs (DRLs).

2.2. Visualization of differentially expressed DRLs in STAD

The analysis of differentially expressed DRLs between gastric cancer and its corresponding normal tissues ($n = 32$) was carried out utilizing the limma package [13]. DRLs that exhibited a notable distinction in expression levels within gastric cancer were identified employing a cutoff of $|\log FC| \geq 1$ and false discovery rate (FDR) adjusted p-value <0.05. To visually represent the differential expression patterns of lncRNAs, a heatmap and a volcano plot were generated.

2.3. Construction and Validation of prognostic-related DRLs model in STAD

Within the scope of this study, the STAD cohort was randomly divided into two sets, namely a training set and a validation set, maintaining a balanced 1:1 ratio. Univariate and multivariate Cox regression analyses were conducted to identify potential prognostic-related DRLs (long non-coding RNAs) in STAD [15]. DRLs exhibiting a p-value <0.05 were considered as candidate prognostic lncRNAs and subjected to subsequent analysis. Furthermore, lasso regression analysis using the glmSparseNet package [16] was performed to address any issues related to overfitting. The final risk model was defined by the equation riskscore = 0.576686042623288 *

IL10RB-DT expression +0.682432842250547 * AL139147.1 expression. Utilizing this novel 2-DRLs risk score model, the risk score was calculated for each sample within the STAD cohort. Based on a cut-off value of 1:1, the TCGA-STAD samples were divided into low-risk and high-risk groups. To assess the predictive efficacy and accuracy of this model for STAD prognosis, Kaplan-Meier survival analysis and Receiver Operating Characteristic (ROC) analysis were conducted. Furthermore, the prognostic evaluation of the 2-DRLs model was validated using both the validation dataset and the entire dataset.

2.4. Differential expression analysis and functional enrichment analysis between high-risk and low-risk groups

To perform differential expression analysis between the high-risk and low-risk subgroups in STAD, the limma package [13] can be utilized. A threshold of $|\log FC| > 1$ and FDR adjusted p-value <0.05 can be employed to select differentially expressed genes (DEGs) among the subgroups. The results of the differential expression analysis can be visually represented using volcano plots and cluster heatmaps.

To explore the molecular mechanisms underlying the differences between the high-risk and low-risk subgroups, Gene Ontology (GO) analysis [17], including GO Biological Process (GO BP), GO Cellular Component (GO CC), and GO Molecular Function (GO MF), as well as KEGG pathway analysis [18], can be performed utilizing the clusterProfiler package [19] in R. The enrichment analysis results can be visualized using bubble plots to display the top 30 enriched terms.

Additionally, Gene Set Enrichment Analysis (GSEA) [20] can be conducted to assess potential biological functional changes between the high-risk and low-risk subgroups. A significance threshold of an absolute value of normalized enrichment score (NES) > 1 and a nominal p-value <0.05 can be applied.By performing these analyses, differentially expressed genes and enriched pathways/processes can be identified, aiding in the elucidation of potential molecular mechanisms associated with the risk stratification in STAD.

2.5. The development and validation of the nomogram

We the survival [16], regplot [16] and rms [16] packages to develope a nomogram for predicting the 3-year and 5-year overall survival (OS) of STAD patients based on risk scores and other clinical indicators.

2.6. Evaluate the role of DRL properties in the STAD immune microenvironment

In order to predict the relative levels of tumor-infiltrating immune cells (TIIC) in the two risk groups based on DRLs features, several algorithms were utilized, including single-sample GSEA (ssGSEA) [21], TIMER [21], QUANTISEQ [21], MCP Counter [21], Estimation [21], EPIC [21], and CIBERSORT [21]. Heatmaps were used to visualize the differences in TIIC concentrations under these different algorithms. Additionally, TIMER was employed to assess the correlation between LMR-lncRNA features and TIIC abundance, aiming to determine the potential impact of DRLs features on immune characteristics. This analysis helps to understand how the identified DRLs may influence the composition of immune cells within the tumor microenvironment, providing insights into the potential role of these features in modulating immune responses in STAD.

2.7. Evaluate the role of DRLs characteristics in STAD chemotherapy drug sensitivity

In R, the pRRophetic [16] and ggplot2 [16] packages can be utilized to perform the Wilcoxon signed-rank test, which is useful for evaluating the drug sensitivity of several anticancer drugs recommended for STAD treatment [22].

2.8. Identification of STAD subtypes in risk prediction models

To identify subtypes of STAD in a risk prediction model, the ConsensusClusterPlus package can be utilized for unsupervised consensus clustering [23]. Using this package, we can set the number of iterations to 50 and the resampling rate to 80%. The consensus cumulative distribution function (CDF) plot, consensus matrix (CM), and consensus heatmap generated by the ConsensusClusterPlus package can be helpful in determining the optimal number of clusters for STAD subtyping. The CDF plot provides information about the stability of the clustering results for different numbers of clusters. The CM shows the consensus clustering results as a matrix, indicating how often pairs of samples are grouped together across iterations. The consensus heatmap provides a visualization of the consensus matrix, allowing for better interpretation of the clustering results. By analyzing these outputs, we can determine the optimal number of clusters for subtyping STAD based on the risk prediction model.

2.9. Statistical analysis

All statistical analyses were performed using R programming language v4.2.1 [24]. To compare the differences in patient survival rates between two risk groups, KM analysis was conducted in conjunction with the log-rank test from the “survival” package in R. Cox proportional hazards regression models were used for both multivariate and univariate analyses to determine the prognostic significance of DRLs features. GSEA analysis was performed to differentiate the two risk groups based on functional annotation. The kruskal test was used to examine differences in immune scores, immune checkpoint gene expression and drug sensitivity in different clusters. Statistical tests were two-sided, and FDR adjusted p-value <0.05 was considered statistically significant.

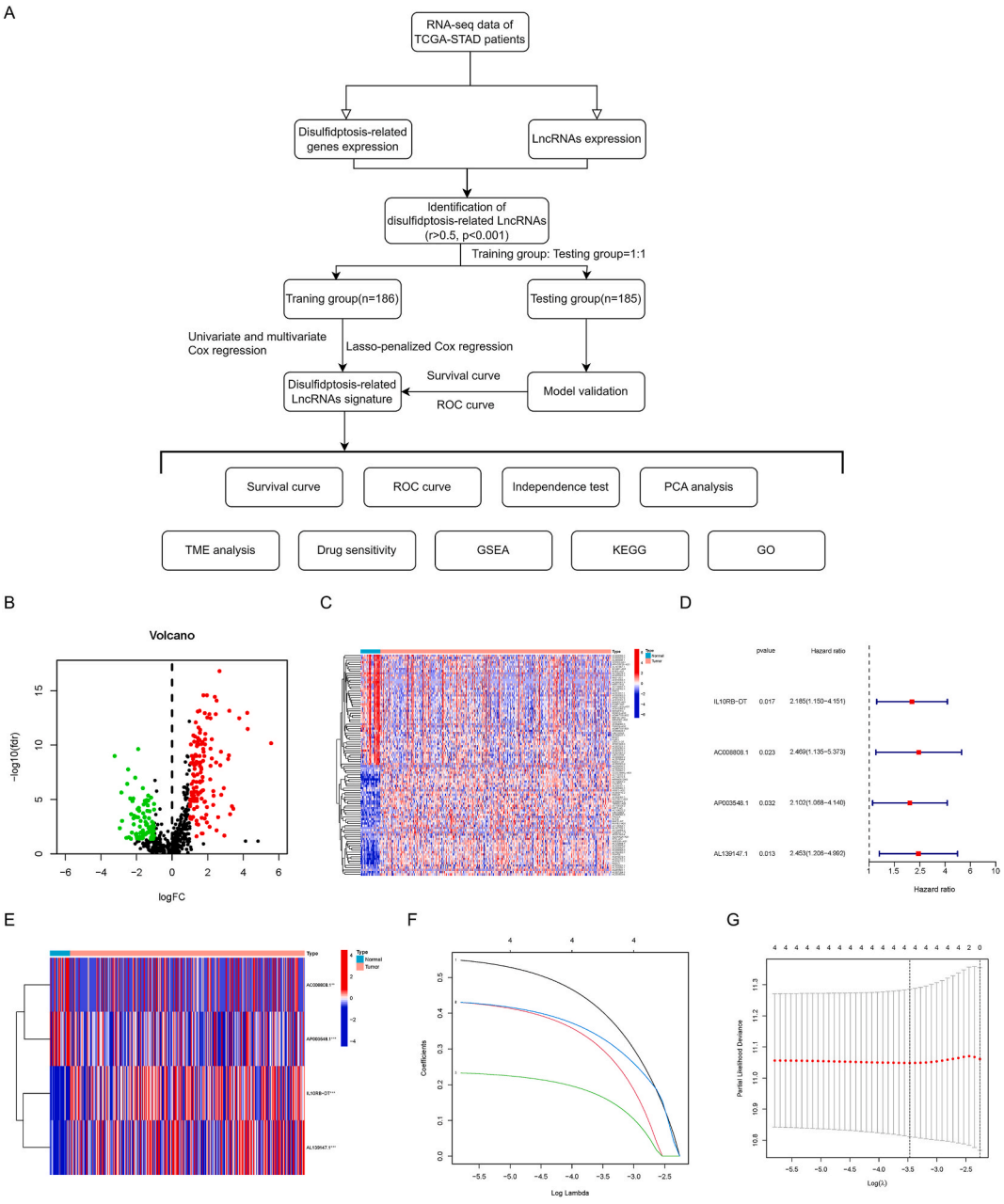

Fig. 1. Identification of prognostic-related DRLs A) Our detailed process flowchart depicts the step-by-step screening and identification of differentially regulated genes (DRLs) that are directly associated with prognosis. B) The visually compelling volcano plot effectively captures and illustrates the distribution of differentially expressed DRLs, enabling a clear representation of their significance. Red: logFC >1, FDR adjusted $p < 0.05$; green: logFC <1, FDR adjusted $p < 0.05$. C) The informative heatmap provides a visual representation of the expression levels of the identified differential DRLs across various samples, allowing for easy comparison and identification of patterns. D) The comprehensive forest plot displays the hazard coefficients of the prognosis-related DRLs, offering a concise and organized overview of their impact on prognosis. E) The heatmap further enhances our understanding by representing the expression levels of the identified prognosis-related DRLs specifically in each individual sample, revealing unique expression profiles. F, G) Through the use of Lasso regression, we are able to effectively demonstrate the potential overfitting situation, showcasing the impact of varying gene counts and highlighting the extent of overfitting within our model. This analysis allows for a better selection and understanding of the most informative genes in relation to the desired outcome.
$^*p < 0.05$, $^{**}p < 0.01$, $^{***}p < 0.001$. (For interpretation of the references to colour in this figure legend, the reader is referred to the Web version of this article.)

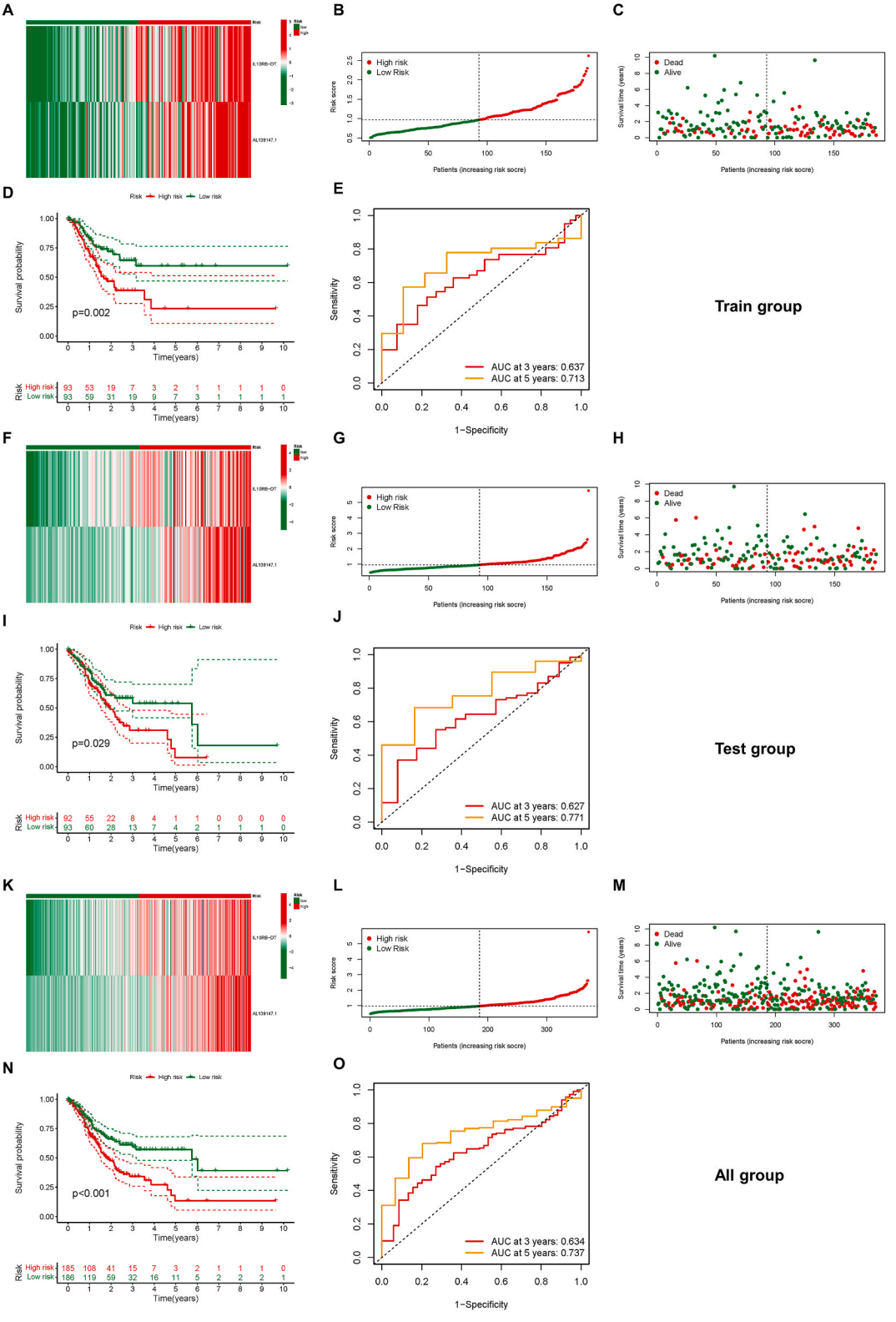

(caption on next page)

Fig. 2. Construction and Validation of DRLs Prognostic Model A) Distribution of risk scores and outcomes in the training set. B) Distribution of risk scores, survival time, and survival status in the training set. C) Expression distribution of five DRL models in patients of the training set. D) Survival curves for patients with different risk scores in the training set. E) ROC curves and area under the curve (AUC) for models in the training set. F) Distribution of risk scores and outcomes in the test set. G) Distribution of risk scores, survival time, and survival status in the test set. H) Expression distribution of five DRL models in patients of the test set. I) Survival curves for patients with different risk scores in the test set. J) ROC curves and AUC for models in the test set. K) Distribution of risk scores and outcomes in all patients. L) Distribution of risk scores, survival time, and survival status in all patients. M) Expression distribution of five DRL models in all patients. N) Survival curves for patients with different risk scores in all patients. O) ROC curves and AUC for models in all patients.
*p < 0.05, **p < 0.01, ***p < 0.001.

3. Results

3.1. Identifying differences in DRLs in the evaluation of STAD

Using the workflow shown in Fig. 1A, we analyzed transcriptomic data from 408 STAD patients' gastric cancer samples. We applied Ensembl's annotation file to annotate and extract mRNA and lncRNA expression. Following previous studies, we extracted expression data for 24 disulfidptosis-related genes (DRGs). Through correlation analysis, we identified 693 disulfidptosis-related lncRNAs (DRLs) with significant expression ($r > 0.5$, $p < 0.001$). We then extracted 89 downregulated and 136 upregulated genes in STAD based on their differential expression compared to paired adjacent tissues ($|\log FC| > 1$, FDR adjusted $p < 0.05$), as shown in Fig. 1B. The top 50 genes with the largest $|\log FC|$ values were visualized in a heatmap (Fig. 1C).

3.2. Construction and validation of a prognostic model for STAD based on DRLs

To predict the prognosis of STAD using 225 DRLs, we divided 371 STAD patients with complete survival information into a training set (n = 186) and a testing set (n = 185) in a 1:1 ratio. In the training set, we performed univariate Cox regression analysis and identified four DRLs associated with prognosis. The relative risk coefficients and expression levels of each DRL in STAD samples are shown in Fig. 1D and E. Next, we used lasso regression to confirm that these four DRLs were included in the prognostic model without overfitting (Fig. 1F and G).

Furthermore, the four DRLs screened based on lasso regression were further subjected to multivariate Cox regression analysis, and we identified two independent prognostic DRLs (IL10RB-DT and AL139147.1) to construct the final STAD prognostic model (Fig. S1). The riskscore was calculated as follows: riskscore = 0.576686042623288 * IL10RB-DT expression +0.682432842250547 * AL139147.1 expression. Based on the riskscore, the training set was divided into high or low-risk groups. Fig. 2A shows the expression levels of different DRLs in the high or low-risk groups, while Fig. 2B and C display the distribution and survival status of STAD patients

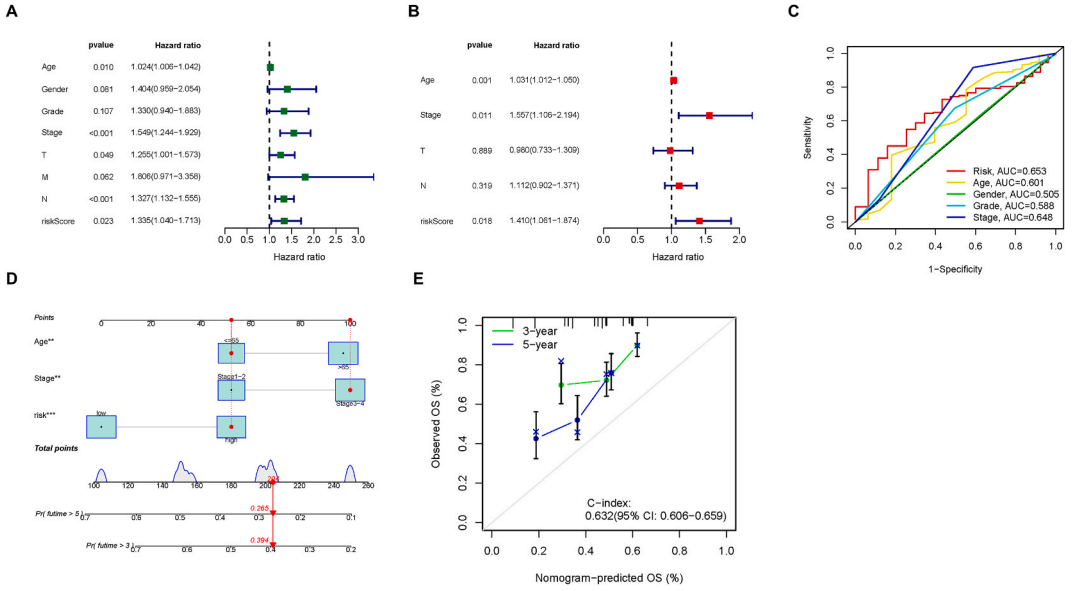

Fig. 3. Association of Prognostic Models and Clinical Factors A) Univariate Cox regression demonstrates the impact of riskscore and other clinical factors on STAD prognosis. B) Multivariate Cox regression evaluates whether riskscore and other clinical factors can serve as independent prognostic factors for STAD. C) Multivariate ROC curves assess the predictive accuracy of riskscore and other clinical factors for STAD prognosis. D) Nomogram establishes specific scoring criteria for evaluating STAD prognosis. E) The C-index curve evaluates the effectiveness of the forest plot.
*$p < 0.05$, **$p < 0.01$, ***$p < 0.001$.

in these groups. The high-risk group demonstrated worse prognosis in survival analysis compared to the low-risk group (Fig. 2D). The ROC curve of the 2-DRLs model exhibited mediocre efficacy with AUC values of 0.637 and 0.731 for 3 and 5 years, respectively (Fig. 2E). Validation using the testing set and the entire STAD dataset yielded similar results in terms of DRL expression, survival analysis, and ROC curve (Fig. 2F-O).

3.3. Clinical correlation analysis of the 2-DRL model

To assess the clinical value of the 2-DRL model, we assumed the riskscore as a prognostic factor for STAD and performed univariate Cox regression analysis with clinical features. We found that only age, stage, T stage, N stage, and riskscore could serve as prognostic factors for STAD (HR > 1, $p < 0.05$) (Fig. 3A). Subsequently, we conducted multivariate Cox regression analysis with these significant prognostic factors, and age, stage, and riskscore demonstrated independent prognostic properties (Fig. 3B). Moreover, when combining these main clinical factors for ROC analysis, riskscore showed the strongest efficacy (Fig. 3C).

Additionally, we constructed nomogram using the meaningful prognostic factors obtained from multivariate Cox regression analysis to assist clinical decision-making (Fig. 3D). The column charts displayed high accuracy and credibility (Fig. 3E). Furthermore, we performed subgroup analyses based on major clinical factors. We found that riskscore had good predictive efficacy for the prognosis of STAD patients, regardless of age (≤65 or >65) [16], early or advanced stage based on grade and stage, and in female patients (Fig. 4A–H). While there was a trend of high riskscore associated with poor prognosis for male patients, it did not reach statistical significance ($p = 0.17$) (Fig. 4C).

3.4. Enrichment analysis and pathway analysis of the high-risk and low-risk groups

To investigate the possible mechanisms underlying the poor prognosis of the high-risk group, we conducted differential analysis and identified 1316 differentially expressed genes ($|logFC| > 1$, FDR adjusted $p < 0.05$) between the high-risk and low-risk groups (Fig. 5A). A heatmap generated by clustering analysis visualized the top 50 genes with the highest logFC values (Fig. 5B). KEGG enrichment analysis revealed enrichment of multiple cancer-related pathways in the high-risk group, including the PI3K-Akt signaling pathway, cGMP-PKG signaling pathway, and Rap1 signaling pathway (Fig. 5C). GO enrichment analysis showed significant changes in cell essential structures such as extracellular matrix organization and membrane microdomain in the high-risk group (Fig. 5D and E). Furthermore, based on the riskscore of each sample, gene set enrichment analysis (GSEA) identified enrichment of the CALCIUM_SIGNALING_PATHWAY in the high-risk group, while the low-risk group showed enrichment of KEGG_GLYCEROLIPID_METABOLISM (Fig. 5F and G). This suggests that calcium signaling pathway dysregulation and altered glycerolipid metabolism may play a role in the respective prognosis groups.

3.5. Assessment of the immune microenvironment in the high-risk and low-risk groups

The occurrence of STAD is closely correlated with the immune microenvironment. We performed calculations for ESTIMATE score, ImmuneScore, and StromalScore in each STAD sample and observed consistent higher values in the high-risk group (Fig. 6A–C). Additionally, the analysis of immune cell infiltration and immune function using single-sample gene set enrichment analysis (ssGSEA)

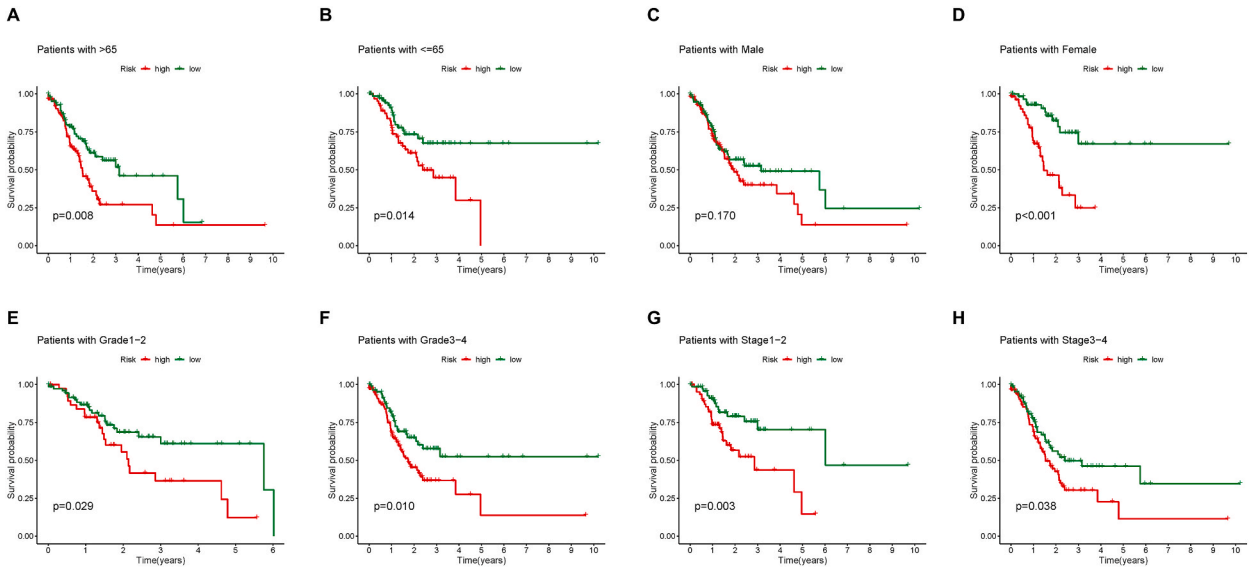

Fig. 4. Riskscore-based survival curves in clinical subgroups A-H) Survival curves based on riskscore in different clinical subgroups.

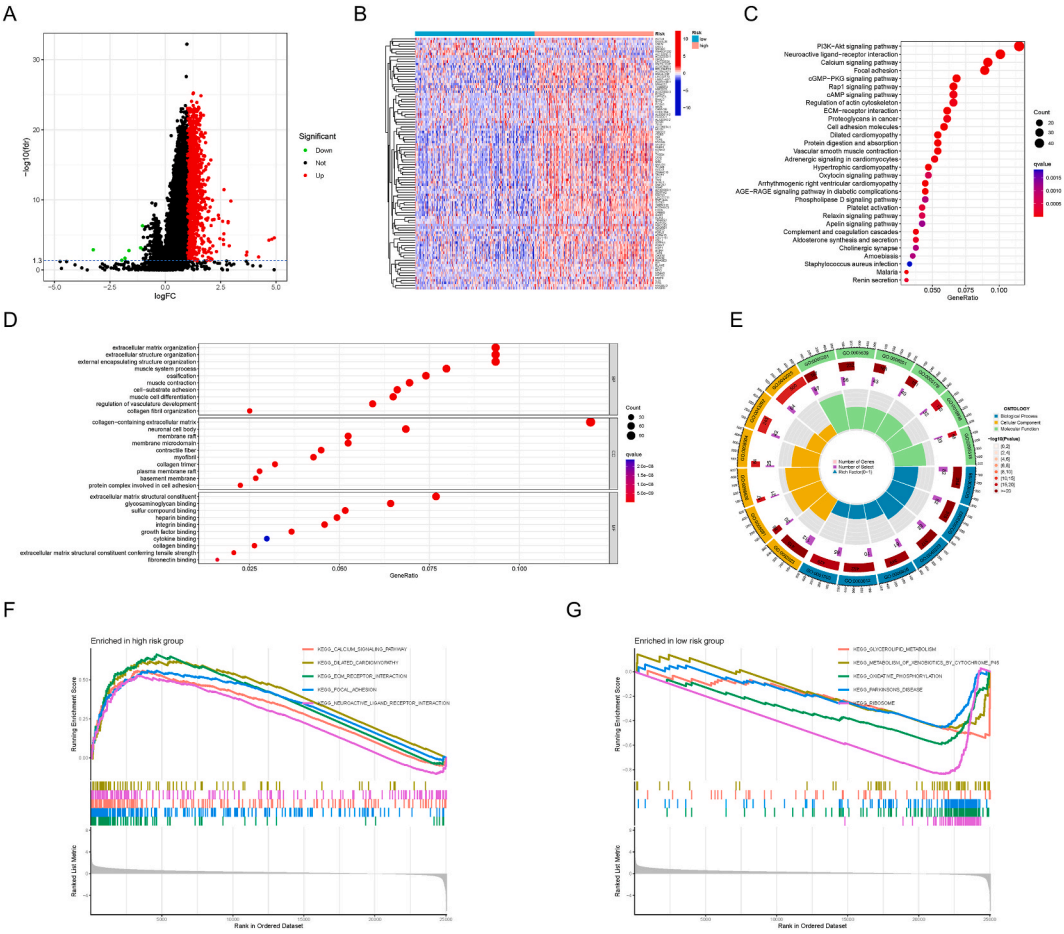

Fig. 5. Functional enrichment analysis based on risk score A) Distribution of differentially expressed genes between high-risk and low-risk groups. Red: logFC >1, FDR adjusted p < 0.05; green: logFC <1, FDR adjusted p < 0.05. B) Expression distribution of differentially expressed genes in high-risk or low-risk groups. C) KEGG enrichment analysis reveals enriched KEGG pathways for differentially expressed genes. D) Bubble plot displays enriched GO pathways for differentially expressed genes. E) Circos plot visualizes the upregulated or downregulated status of differentially expressed genes in GO pathways. F) GSEA analysis showcases highly expressed pathways in the high-risk group. G) GSEA analysis demonstrates lowly expressed pathways in the low-risk group.
*$p < 0.05$, **$p < 0.01$, ***$p < 0.001$. (For interpretation of the references to colour in this figure legend, the reader is referred to the Web version of this article.)

revealed increased infiltration of all immune cells and enhanced immune responses in the high-risk group (Fig. 6D and E). Furthermore, we explored the correlation between various immune cell infiltrates and riskscore using algorithms such as ssGSEA, TIMER, QUANTISEQ, MCP counter, ESTIMATE, EPIC, and CIBERSORT. T cell $CD4^+$ cells exhibited a robust positive correlation with riskscore across all algorithms (Fig. 6F). Concerning the association between immune cell infiltration and STAD prognosis, we found a significant connection between high levels of macrophage infiltration and poor prognosis in STAD patients (Fig. 6G), while high levels of T cell follicular helper cells showed the opposite effect (Fig. 6H). Moreover, we assessed the expression levels of immune checkpoint genes in the high-risk and low-risk groups. Surprisingly, nearly all immune checkpoint genes showed high expression in the high-risk group (Fig. 6I). These findings suggest that although the high-risk group mobilizes a large number of immune cells, the high expression of immune checkpoint genes in their microenvironment inhibits the anti-tumor function of these immune cells, leading to a poor prognosis in high-risk group patients.

3.6. Assessment of chemotherapy drug sensitivity in the high-risk and low-risk groups

Since chemotherapy is the main treatment modality for gastric cancer, and drug resistance is highly prevalent, we aimed to utilize a 2-DRL model to guide clinical chemotherapy regimens and improve the cure rate of STAD patients. We employed the pRRophetic algorithm to evaluate the chemotherapy drug sensitivity in the high-risk and low-risk groups. Our analysis revealed that patients in the high-risk group exhibited better sensitivity to Erlotinib, Oxaliplatin, and Gefitinib (Fig. 6J-L). Targeted therapy with these drugs may potentially improve the prognosis of high-risk group patients.

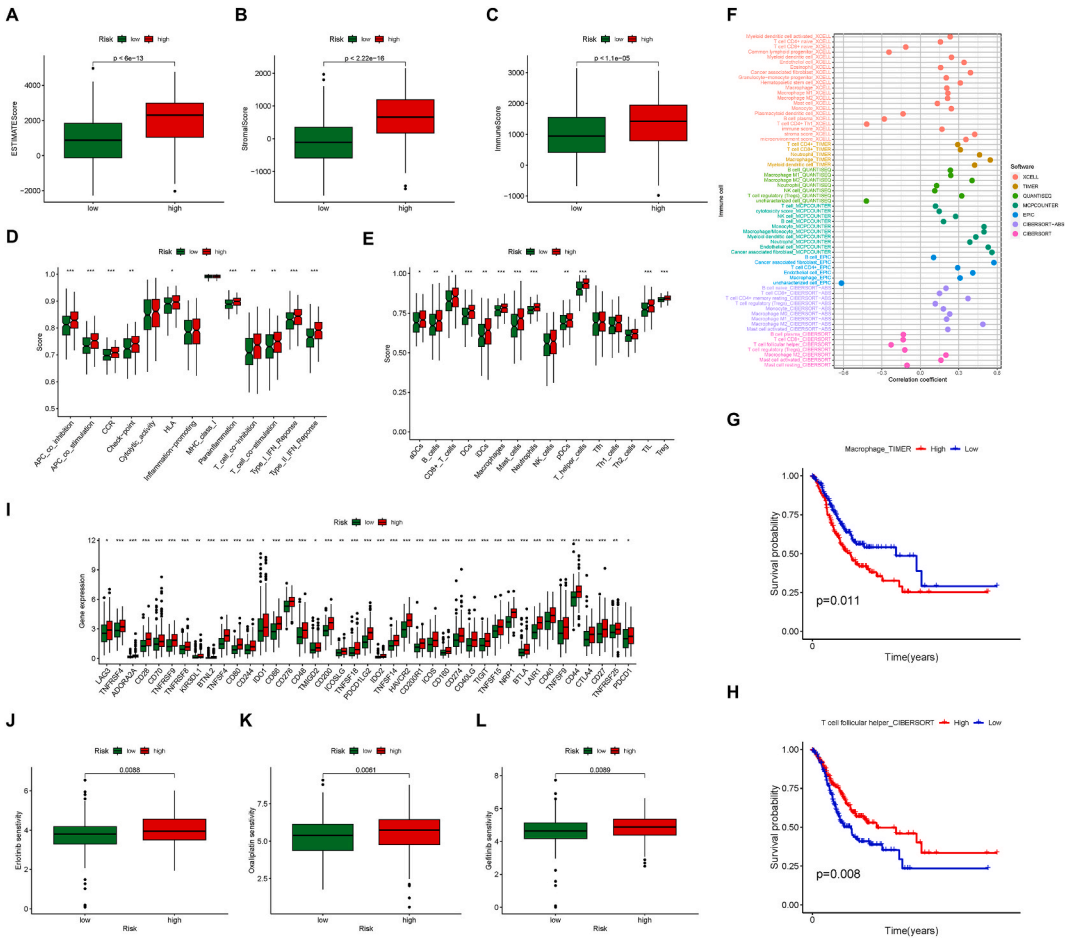

Fig. 6. Immune status and drug sensitivity in different risk score groups A-C) STAD tumor microenvironment score. D) Immune function status in different risk score groups. E) Immune cell infiltration patterns in different risk score groups. F) Quantitative analysis of immune cell infiltration in STAD tissues using various algorithms such as XCELL, TIMER, QUANTISEQ, MCPCOUNTER, EPIC, CIBERSORT-ABS, and CIBERSORT. G, H) Survival curves based on different immune cell infiltration scores. I) Expression of immune checkpoints in different risk score groups. J-K) Drug sensitivity profiles in different risk score groups.
$^{*}p < 0.05$, $^{**}p < 0.01$, $^{***}p < 0.001$.

3.7. The novel molecular subtyping of STAD based on the 2-DRL model

We attempted to perform molecular subtyping of STAD using the 2-DRL model. We utilized Consensus Cluster Plus to identify different subtypes within the risk model (K = 2–9). Based on the cumulative distribution function (CDF) curves and Delta area display (Fig. 7A and B), when k = 2 or 3, the sample clusters showed good stability (Fig. 7C and D). However, when k = 2, the distribution of patients in the molecular subtypes was similar to the classification based on risk scoring (Fig. 7E), whereas k = 3 represented a completely new molecular subtype (Fig. 7F). PCA and tSNE analysis demonstrated that both the high-risk and low-risk groups, as well as the k = 3 molecular subtypes, could effectively differentiate different STAD patients (Fig. 7G–J). Moreover, survival analysis revealed that patients in the C2 group had the poorest prognosis, while there was no significant difference between the C1 and C3 groups (Fig. 7K).

Immunological microenvironment and chemotherapy resistance evaluation of the new molecular subtypes in STAD.

Next, we evaluated the immunological microenvironment characteristics of the new molecular subtypes in STAD. We found that patients in the C2 group had higher ESTIMATEScore, ImmuneScore, and StromalScore (Fig. 8A–C) and exhibited independent activation of 12 immune checkpoint genes (Fig. 8D, Fig. S2), which corresponded to the poor prognosis observed in the C2 group (Fig. 7K). The clustering heatmap revealed that in terms of immune cell infiltration, patients in the C2 group showed the highest levels of immune cell infiltration, followed by the C1 and C3 groups (Fig. 8E). Regarding chemotherapy drug sensitivity, patients in the C2 group demonstrated better sensitivity to Erlotinib, Cisplatin, Oxaliplatin, and Gefitinib. Additionally, the C3 group exhibited good sensitivity to Cisplatin. There were no significant differences between the C1 and C3 groups in terms of sensitivity to Erlotinib, Oxaliplatin, and Gefitinib (Fig. 8F–I).

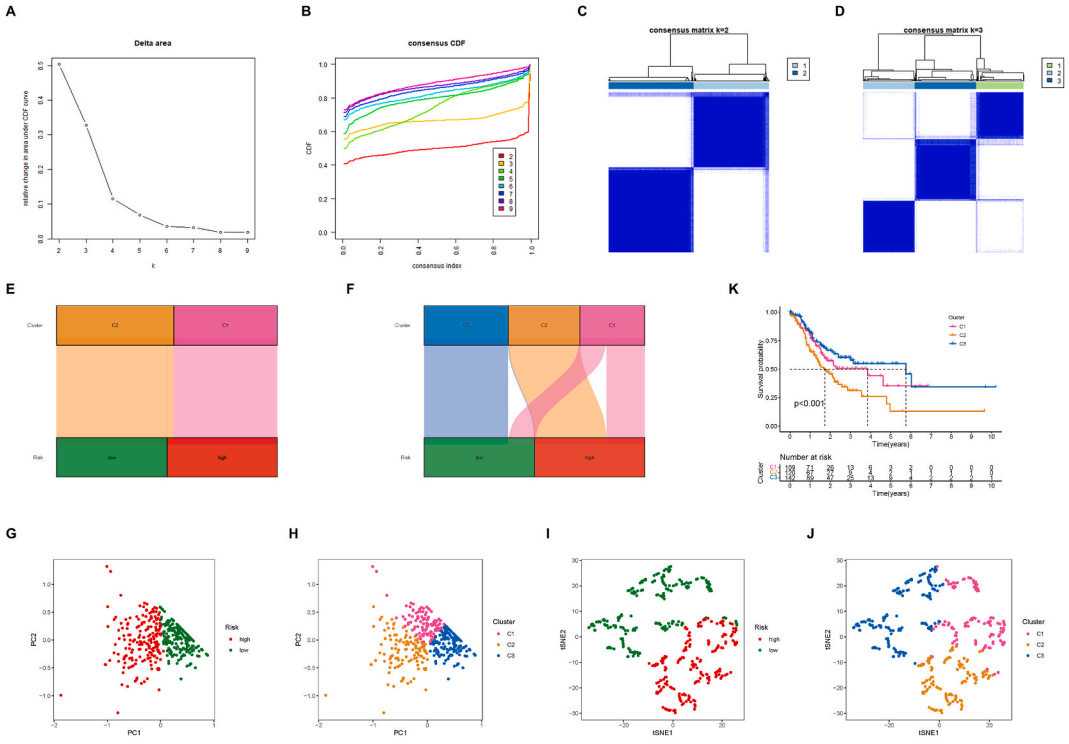

Fig. 7. Classification of STAD subtypes based on DRLs model genes A) Distribution of samples across different number of classifications. B) CDF curves for different number of classifications. C) Consensus matrix for 2 classifications. D) Consensus matrix for 3 classifications. E, F) Sankey diagram illustrating the correspondence between STAD subtypes and high/low-risk score groups. G)PCA analysis showing the distribution of samples across different risk score groups. H)PCA analysis showing the distribution of samples across different STAD subtypes. I)t-SNE analysis showing the distribution of samples across different risk score groups. J)t-SNE analysis showing the distribution of samples across different STAD subtypes. K)Survival curves for different STAD subtypes.
$^{*}p < 0.05$, $^{**}p < 0.01$, $^{***}p < 0.001$.

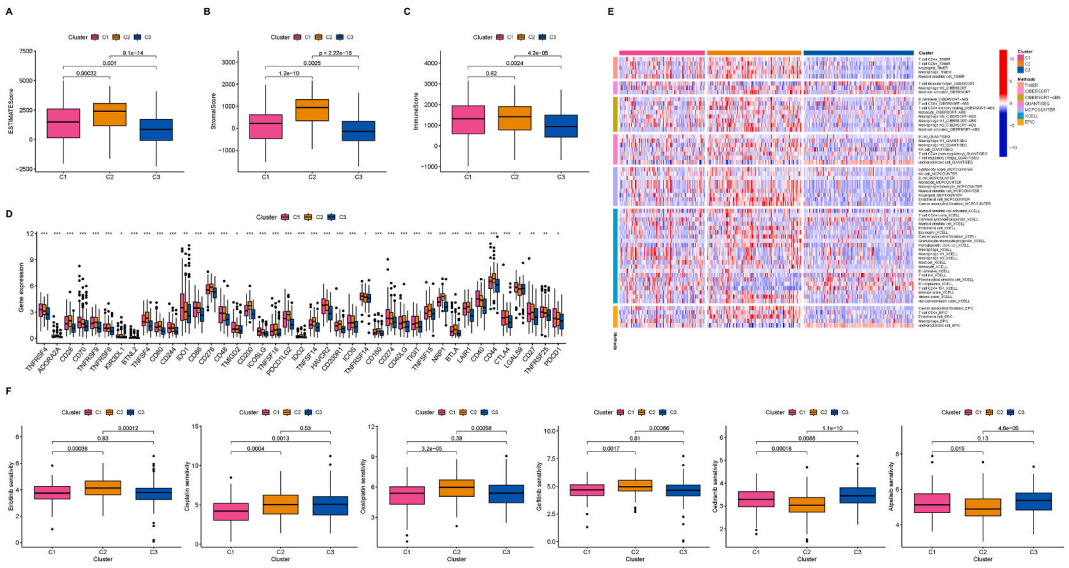

Fig. 8. Immune status and drug sensitivity in different STAD subtypes A-C) Estimatescore, stromalscore and immunescore in different STAD subtypes. D) Expression of immune checkpoints in different STAD subtypes. E) Quantitative analysis of immune cell infiltration in STAD tissues using various algorithms such as XCELL, TIMER, QUANTISEQ, MCPCOUNTER, EPIC, CIBERSORT-ABS, and CIBERSORT. F) Drug sensitivity profiles in different STAD subtypes.

4. Discussion

Cell death, a physiological process crucial for maintaining biological development and internal homeostasis, has become a focus in cancer treatment as targeting cell death-related pathways can effectively eliminate cancer cells [25,26]. Recently, a team of researchers made a significant discovery and characterization of a novel form of cell death known as Disulfidptosis. This finding has opened up new possibilities for cancer therapy [7]. However, its role in stomach adenocarcinoma (STAD) remains largely unexplored. In this study, we aimed to investigate the relevance of Disulfidptosis-related genes (DRLs) in STAD by employing correlation analysis. Furthermore, we constructed a 2-DRLs prognostic model utilizing univariate Cox regression, LASSO regression, and multivariate Cox regression. Our analysis demonstrated that patients categorized in the high-risk group exhibited significantly shorter overall survival compared to those in the low-risk group. Moreover, through the visualization of risk heatmaps, risk curves, receiver operating characteristic (ROC) curves, and Kaplan-Meier survival curves, we corroborated the strong predictive efficacy of our risk model, surpassing other crucial risk factors in STAD, including age and stage. Notably, similar robust results were obtained in the validation set, further validating the reliability and reproducibility of our findings.

STAD tumors thrive within a complex tumor microenvironment that aids in promoting malignant tumor progression and evading immune defenses [27,28]. Recent breakthroughs in immunotherapy have uncovered the potential of targeting immune regulatory cells or immune checkpoint factors within the tumor microenvironment to elicit anti-tumor immune responses [29,30]. Notably, Disulfidptosis has been shown to have close associations with the tumor immune microenvironment [31]. Additionally, emerging evidence suggests that aberrant long non-coding RNAs (lncRNAs) play a significant role as novel markers contributing to anti-tumor immune responsiveness [11,32,33]. Therefore, comprehending the tumor immune microenvironment influenced by Disulfidptosis-related genes (DRLs) and identifying new markers is crucial for effective risk stratification and target selection in immune therapy. In our study, we observed elevated levels of various immune cell infiltrates in the high-risk group, accompanied by higher ESTIMATEScore, ImmuneScore, and StromalScore compared to the low-risk group. These findings imply immune tolerance in high-risk STAD patients. Consequently, the features of DRLs hold potential as valuable indicators for selecting more efficient anti-tumor immune therapies for patients. However, further validation is necessary to fully comprehend the role of these features in predicting the immune treatment response of STAD patients.

Immune checkpoints refers to a series of molecules expressed on immune cells that can regulate the degree of immune activation [34]. They play a crucial role in preventing autoimmune responses (abnormal immune function attacking normal cells) [35]. Currently, there are many drugs targeting immune checkpoints that have shown promising results in clinical treatment of some STAD patients [36]. However, they are still ineffective for many patients [37]. We found that all immune checkpoint genes were upregulated in the high-risk group, indicating immune suppression and decreased immune response against tumors in these patients. Regarding IL10RB-DT and AL139147.1 in the 2-DRLs prognostic model, it has been reported that IL10RB-DT inhibits $CD8^+$ T cell activation by suppressing IFN-γ-JAK-STAT1 signaling and antigen presentation in melanoma and breast cancer cells [38], which may be related to the activation of immune checkpoints found in our analysis. As for AL139147.1, it has not been studied yet. Future in-depth research on IL10RB-DT and AL139147.1 may lead to effective treatment targets for immune checkpoints.

Chemotherapy is the main treatment for STAD, and drug resistance is a major challenge in curing gastric cancer [39]. Using the pRRophetic algorithm, we evaluated the chemosensitivity of high-risk and low-risk patients and found that high-risk patients have better sensitivity to Erlotinib, Oxaliplatin, and Gefitinib, which can help in clinical decision-making and improve patient prognosis. Additionally, IL10RB-DT and AL139147.1 may also serve as important targets to improve drug sensitivity in STAD.

In addition to identifying candidate biomarkers in STAD, finding precise molecular subtypes is also crucial for improving personalized treatment [40,41]. Based on the 2-DRLs prognostic model, we were able to classify STAD patients into three molecular subtypes (C1, C2, and C3). We then evaluated subtype-specific prognostic values, immune infiltration, and chemosensitivity. Our results showed that C1 and C3 patients had the best prognosis, C2 patients had the worst prognosis. In terms of the immune microenvironment, C2 patients exhibited significant immune infiltration, while C3 patients had less immune cell infiltration, and C1 patients were intermediate. Drug sensitivity analysis indicated that C2 patients showed better sensitivity to Alpelisib and Cediranib, C1 patients were more suitable for treatment with Erlotinib, Cisplatin, Oxaliplatin, and Gefitinib, while C3 patients were more suitable for Erlotinib, Oxaliplatin, and Gefitinib treatment. Our novel STAD molecular subtyping holds significant implications for precise treatment of STAD.

This study still has certain limitations. One of them is that we have not identified the reasons for better prognosis in the C1 group. Despite the similarity in patient prognosis between the C1 and C3 groups, there are significant differences in the immune microenvironment. These findings suggest that there may be other important factors contributing to the improved prognosis of patients in the C1 group, which represents an area for future in-depth research. Another limitation of this study is All the ranges and points of the nomogram we constructed are above the 45-degree line, which is an indication that the predicted values have a lower survival probability than the observation in reality. This may be due to the smaller overall sample size of STAD, which is needed in the future. More data will be collected for nomogram training and optimization. In addition, more evaluation indicators should be tried in subsequent work to make it more practical and clinically applicable. The lack of external validation for our 2-DRL model, as we lacked a comprehensive survival dataset from external lncRNA datasets. Improving the clinical information in large-scale lncRNA datasets in the future can assist us in further validating our model.

5. Conclusion

In summary, we analyzed and identified DRLs features in STAD. The 2-DRL model demonstrated satisfactory performance in

predicting OS differences and revealed the heterogeneity of the immune microenvironment in STAD patients. Additionally, the 2-DRL model can guide precise drug selection for chemotherapy in different molecular subtypes of STAD patients, improving treatment effectiveness and overcoming drug resistance. The robust and powerful DRL risk model provides insightful recommendations for exploring better treatment decisions and studying the mechanisms of DRLs.

Funding

This work was supported by the National Natural Science Foundation of China (8236030102) and the Yunnan Provincial Department of Science and Technology Kunming Medical Joint Special Project (202301AY070001-025).

Ethics statement

Not appilicatable.

Consent for publication

Not appilicatable.

Data availability statement

The results published here are in whole based upon data generated by the TCGA Research Network: https://www.cancer.gov/tcga. All other relevant data can be found in the supplementary material and will be made available on request.

CRediT authorship contribution statement

Jinze Li: Writing – review & editing, Writing – original draft, Visualization, Validation, Methodology, Conceptualization. **Chuqi Xia:** Writing – review & editing, Writing – original draft, Validation, Resources, Methodology, Conceptualization. **Yilin Song:** Writing – review & editing, Writing – original draft, Methodology, Conceptualization. **Lu Zhang:** Resources, Methodology, Conceptualization. **Wei Shang:** Visualization, Data curation. **Ning Xu:** Writing – review & editing, Writing – original draft, Methodology. **Qiyu Lu:** Writing – review & editing, Writing – original draft, Validation, Methodology, Investigation, Conceptualization. **Daoming Liang:** Writing – review & editing, Writing – original draft, Supervision, Resources, Methodology, Funding acquisition, Formal analysis, Conceptualization.

Declaration of competing interest

The authors declare that they have no known competing financial interests or personal relationships that could have appeared to influence the work reported in this paper.

Acknowledgments

Not appilicatable.

Appendix A. Supplementary data

Supplementary data to this article can be found online at https://doi.org/10.1016/j.heliyon.2024.e29005.

References

[1] J. Machlowska, et al., Gastric cancer: epidemiology, risk factors, classification, genomic characteristics and treatment strategies, Int. J. Mol. Sci. 21 (11) (2020).
[2] D.E. Guggenheim, M.A. Shah, Gastric cancer epidemiology and risk factors, J. Surg. Oncol. 107 (3) (2013) 230–236.
[3] A.P. Thrift, H.B. El-Serag, Burden of gastric cancer, Clin. Gastroenterol. Hepatol. 18 (3) (2020) 534–542.
[4] J. Poorolajal, et al., Risk factors for stomach cancer: a systematic review and meta-analysis, Epidemiol Health 42 (2020) e2020004.
[5] X. Liu, L. Zhuang, B. Gan, Disulfidptosis: disulfide stress-induced cell death, Trends Cell Biol 34 (4) (2023) 327–337.
[6] X. Liu, et al., Cystine transporter regulation of pentose phosphate pathway dependency and disulfide stress exposes a targetable metabolic vulnerability in cancer, Nat. Cell Biol. 22 (4) (2020) 476–486.
[7] X. Liu, et al., Actin cytoskeleton vulnerability to disulfide stress mediates disulfidptosis, Nat. Cell Biol. 25 (3) (2023) 404–414.
[8] R. Sun, et al., AADAC protects colorectal cancer liver colonization from ferroptosis through SLC7A11-dependent inhibition of lipid peroxidation, J. Exp. Clin. Cancer Res. 41 (1) (2022) 284.
[9] L. Su, et al., Mitochondria ROS and mitophagy in acute kidney injury, Autophagy 19 (2) (2023) 401–414.
[10] X. Liu, B. Gan, Glucose starvation induces NADPH collapse and disulfide stress in SLC7A11(high) cancer cells, Oncotarget 12 (16) (2021) 1629–1630.
[11] K. Xu, et al., ncRNA-mediated fatty acid metabolism reprogramming in HCC, Trends Endocrinol Metab 34 (5) (2023) 278–291.

[12] C. Liu, et al., LncRNA RP11-620J15.3 promotes HCC cell proliferation and metastasis by targeting miR-326/GPI to enhance glycolysis, Biol. Direct 18 (1) (2023) 15.
[13] K. Xu, et al., A six lipid metabolism related gene signature for predicting the prognosis of hepatocellular carcinoma, Sci. Rep. 12 (1) (2022) 20781.
[14] Y. Yan, et al., SLC7A11 expression level dictates differential responses to oxidative stress in cancer cells, Nat. Commun. 14 (1) (2023) 3673.
[15] F. Xing, et al., Construction of a novel disulfidptosis-related lncRNA prognostic signature in pancreatic cancer, Mol. Biotechnol. (2023).
[16] K. Xu, et al., Disulfidptosis-related lncRNA signatures assess immune microenvironment and drug sensitivity in hepatocellular carcinoma, Comput. Biol. Med. 169 (2024) 107930.
[17] M. Ashburner, et al., Gene ontology: tool for the unification of biology. The Gene Ontology Consortium, Nat. Genet. 25 (1) (2000) 25–29.
[18] M. Kanehisa, S. Goto, KEGG: kyoto encyclopedia of genes and genomes, Nucleic Acids Res. 28 (1) (2000) 27–30.
[19] W. Xue, et al., Disulfidptosis-associated long non-coding RNA signature predicts the prognosis, tumor microenvironment, and immunotherapy and chemotherapy options in colon adenocarcinoma, Cancer Cell Int. 23 (1) (2023) 218.
[20] A. Subramanian, et al., Gene set enrichment analysis: a knowledge-based approach for interpreting genome-wide expression profiles, Proc Natl Acad Sci U S A 102 (43) (2005) 15545–15550.
[21] G. Hu, et al., A bioinformatics approach to identify a disulfidptosis-related gene signature for prognostic implication in colon adenocarcinoma, Sci. Rep. 13 (1) (2023) 12403.
[22] L. Liu, et al., Disulfidptosis-associated LncRNAs index predicts prognosis and chemotherapy drugs sensitivity in cervical cancer, Sci. Rep. 13 (1) (2023) 12470.
[23] B. Sandeep, et al., Insights regarding the article "exploring transthyretin amyloid cardiomyopathy: a comprehensive review of the disease and upcoming treatments", Curr. Probl. Cardiol. 49 (1 Pt B) (2023) 102100.
[24] R.C.T.R. Null, et al., R: a language and environment for statistical computing, Computing 1 (2011) 12–21.
[25] G. Kroemer, et al., Immunogenic cell death in cancer therapy, Annu. Rev. Immunol. 31 (2013) 51–72.
[26] F. Peng, et al., Regulated cell death (RCD) in cancer: key pathways and targeted therapies, Signal Transduct Target Ther 7 (1) (2022) 286.
[27] L. Miao, et al., Targeting the STING pathway in tumor-associated macrophages regulates innate immune sensing of gastric cancer cells, Theranostics 10 (2) (2020) 498–515.
[28] Y. He, et al., Identification of immune-related prognostic markers in gastric cancer, J Healthc Eng 2022 (2022) 7897274.
[29] J. Xie, L. Fu, L. Jin, Immunotherapy of gastric cancer: past, future perspective and challenges, Pathol. Res. Pract. 218 (2021) 153322.
[30] D. Vrana, et al., From tumor immunology to immunotherapy in gastric and esophageal cancer, Int. J. Mol. Sci. 20 (1) (2018).
[31] T. Wang, et al., Disulfidptosis classification of hepatocellular carcinoma reveals correlation with clinical prognosis and immune profile, Int Immunopharmacol 120 (2023) 110368.
[32] F. Wang, et al., Cuproptosis-related lncRNA predict prognosis and immune response of lung adenocarcinoma, World J. Surg. Oncol. 20 (1) (2022) 275.
[33] Z.H. Feng, et al., m6A-immune-related lncRNA prognostic signature for predicting immune landscape and prognosis of bladder cancer, J. Transl. Med. 20 (1) (2022) 492.
[34] B. Li, H.L. Chan, P. Chen, Immune checkpoint inhibitors: basics and challenges, Curr. Med. Chem. 26 (17) (2019) 3009–3025.
[35] S.L. Topalian, et al., Mechanism-driven biomarkers to guide immune checkpoint blockade in cancer therapy, Nat. Rev. Cancer 16 (5) (2016) 275–287.
[36] M.A. Postow, R. Sidlow, M.D. Hellmann, Immune-related adverse events associated with immune checkpoint blockade, N. Engl. J. Med. 378 (2) (2018) 158–168.
[37] Y. Wang, et al., Genome-wide gain-of-function screening characterized lncRNA regulators for tumor immune response, Sci. Adv. 8 (49) (2022) eadd0005.
[38] L. Wei, et al., Noncoding RNAs in gastric cancer: implications for drug resistance, Mol. Cancer 19 (1) (2020) 62.
[39] Z. Chen, et al., Progress and current status of molecule-targeted therapy and drug resistance in gastric cancer, Drugs Today 56 (7) (2020) 469–482.
[40] Q. Zhao, et al., Immunotherapy for gastric cancer: dilemmas and prospect, Brief Funct Genomics 18 (2) (2019) 107–112.
[41] Y.Y. Choi, S.H. Noh, J.H. Cheong, Evolution of gastric cancer treatment: from the golden age of surgery to an era of precision medicine, Yonsei Med. J. 56 (5) (2015) 1177–1185.